Processing of high resolution, multiparametric radar data for the Airborne Dual-Frequency Precipitation Radar APR-2

Simone Tanelli, Jonathan P. Meagher, Stephen L. Durden and Eastwood Im
Jet Propulsion Laboratory, California Institute of Technology, Pasadena CA, USA

ABSTRACT

Following the successful Precipitation Radar (PR) of the Tropical Rainfall Measuring Mission[1], a new airborne, 14/35 GHz rain profiling radar, known as Airborne Precipitation Radar – 2 (APR-2)[2], has been developed as a prototype for an advanced, dual-frequency spaceborne radar for a future spaceborne precipitation measurement mission[3]. This airborne instrument is capable of making simultaneous measurements of rainfall parameters, including co-pol and cross-pol rain reflectivities and vertical Doppler velocities, at 14 and 35 GHz. Furthermore, it also features several advanced technologies for performance improvement, including real-time data processing, low-sidelobe dual-frequency pulse compression, and dual-frequency scanning antenna.

Since August 2001, APR-2 has been deployed on the NASA P3 and DC8 aircrafts in four experiments including CAMEX-4 and the Wakasa Bay Experiment. Raw radar data are first processed to obtain reflectivity, LDR (linear depolarization ratio), and Doppler velocity measurements. The dataset is then processed iteratively to accurately estimate the true aircraft navigation parameters and to classify the surface return. These intermediate products are then used to refine reflectivity and LDR calibrations (by analyzing clear air ocean surface returns), and to correct Doppler measurements for the aircraft motion. Finally, the melting layer of precipitation is detected and its boundaries and characteristics are identified at the APR-2 range resolution of 30m. The resulting 3D dataset will be used for validation of other airborne and spaceborne instruments, development of multiparametric rain/snow retrieval algorithms and melting layer characterization and statistics. In this paper the processing approach is described in detail together with an overview of the resulting data quality and known issues.

Keywords: Precipitation, Airborne Doppler Radar

1. INTRODUCTION

1.1. Radar description

The main parameters of APR-2 radar system are shown in Table 1. The operating frequencies match those planned for the Global Precipitation Mission (GPM), a single reflector antenna, mechanically scanning +/- 25° in cross-track elevation, is under illuminated at Ka band in order to match the beamwidths at the two frequencies. Each cross-track scan is sampled at 24 positions, since January 2003 the 24th position is used for noise floor measurements (i.e., no pulse is transmitted, therefore the +/- 25° range is divided in 23 equally spaced positions). Pulse compression is used to obtain a synthetic pulse width of 60 m (6dB), the radar return signal is then sampled every 0.2 μs, equivalent to 30 m range gates.

TABLE I. APR-2 PARAMETERS

Airborne PR-2 Nominal Parameters		
Frequency	13.4 GHz	35.6 GHz
Polarization	HH,HV	HH,HV
Antenna diameter (effective)	0.4 m	0.14 m
Beamwidth	3.8 deg	4.8 deg
Antenna Gain	34 dBi	33 dBi
Antenna sidelobe level	-30 dB	-30 dB
Polarization Isolation	-25 dB	-25 dB
Peak Power	200 W	100 W
Bandwidth	4 MHz	4 MHz
Pulse Width	10-40 μs	10-40 μs
PRF	5 kHz	5kHz
6dB Pulse Width (after compression)	60 m	60 m
Range Bin Spacing	30 m	30 m
Horizontal res (a/c at 6 km alt)	400 m	500 m
Ground swath (a/c at 6 km alt)	4.5 km	4.5 km
Number of averaged pulses	250	250
Equiv. num. of independent samples	~60	~60
Noise equivalent Z_e (at 10 km range)	5 dBZ	5 dBZ
Doppler precision	0.4 m/s	>1 m/s

Figure 1 shows the observed nadir radar return in clear air and over ocean for both operating frequencies. The Noise floor is here converted in equivalent detectable reflectivity. The values for both Ku-band and Ka-band are below 5 dBZ at 10 km range from the radar; however due to data processor non-linearities the effective minimum detectable reflectivity was approximately 5 dBZ already at 6 km range.

The surface return, along with pulse compression sidelobes can be seen at approximately 6 km range. The pulse compression sidelobes, rather than thermal noise, limit the performance near the surface, -50 dB range sidelobe rejection is achieved in less than 250 m. Achieving such low pulse compression sidelobes required careful design of the transmit waveform and control of gain and phase errors.

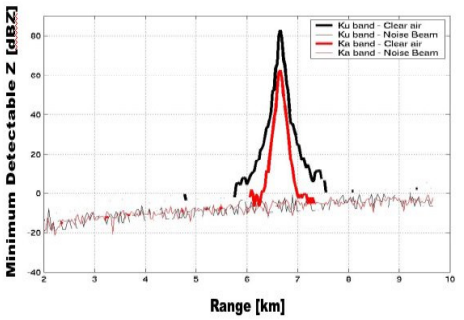

Figure 1. Observed minimum detectable reflectivity. Surface return and pulse compression sidelobes are visibile at around 6.7 km range.

1.2. Calibration

APR-2 data quality has been assessed by examining a number of engineering parameters related to the radar's stability and calibration. Calibration can be verified using observations of the ocean surface in clear air conditions. This technique has been used previously with the Ku-band NASA/JPL airborne precipitation radar ARMAR[4], since the ocean backscatter is well known, especially near 10 degrees incidence, where sensitivity to wind speed has a minimum. Observations of the ocean surface with APR-2 show a Ku band normalized cross section of about 7.1 dB at 10 degrees incidence angle, which is close to previous measurements and models. Ocean backscatter observations from APR-2 in different wind conditions are shown in Fig 2. Comparison with surface reflectivities calculated with Geophysical Model Function (GMF) or from TRMM/PR measurements seem to indicate small a bias of less than ~0.5 dBZ, however strong winds and clouds undetected by APR-2 are possible contributors for this bias at Ku band, in depth analysis is required to further refine calibration.

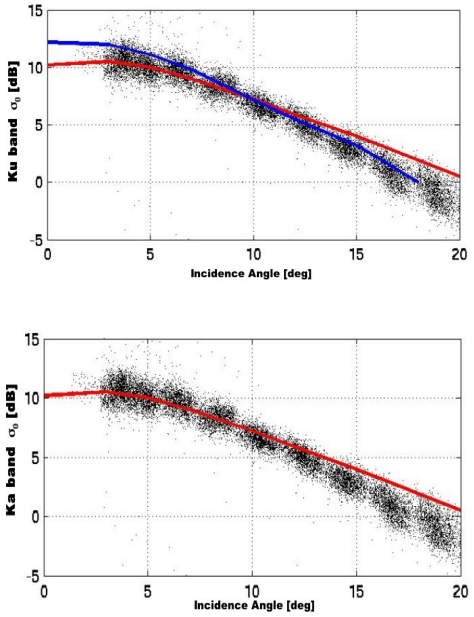

Figure 2. APR-2 observations of ocean backscatter versus incidence angle. Black: APR-2 measurements, Red: GMF, Blue: TRMM/PR global mean

Ocean backscatter at Ka-band is much less well characterized, although models show similar behavior to Ku-band. On the other hand, Ka band reflectivity in very light rain is expected to be nearly identical to that at Ku-band, since Rayleigh scattering should apply at both frequencies. In order to minimize the bias introduced by the different specific attenuation at the two frequencies, Ka-band calibration was verified relatively to Ku band by comparing returns in the top portion of very light rain areas. An automated procedure was developed to select suitable portions of the 3D dataset and extract the statistics of Ka-band reflectivity vs Ku-band reflectivity. This procedure was applied to the whole dataset generated during the Wakasa Bay Experiment conducted in January and February 2003 overall, Ka-band reflectivity measurements in light rain conditions match the corresponding Ku-band measurements with <1 dB rmse (see Figure 3). Selection of appropriate portions of the rainfield was possible only after incorporating three algorithms described in section 3 in the APR-2 processing software (see the diagram in Figure 4).

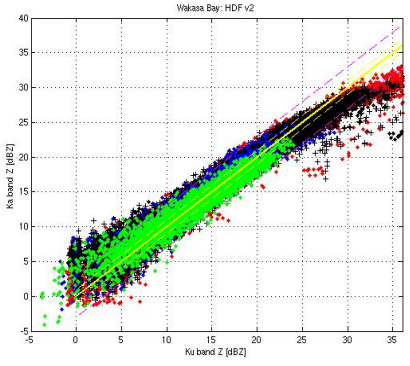

Figure 3. Ka-band calibration relative to Ku-band measurements

In the Wakasa Bay Experiment configuration the cross-polarization leakage at Ka band was larger than nominal (-25 dB). In fact, it was estimated at –17.4 dB through observation of clear air, vertical incidence returns of ocean surface. By removing this leakage the useful range of LDR measurements at Ka band was reduced at about –15 dB. The cross-polarization leakage of the Ku band channel was at nominal values, hence LDR measurements at Ku band as low as –25 dB were obtained.

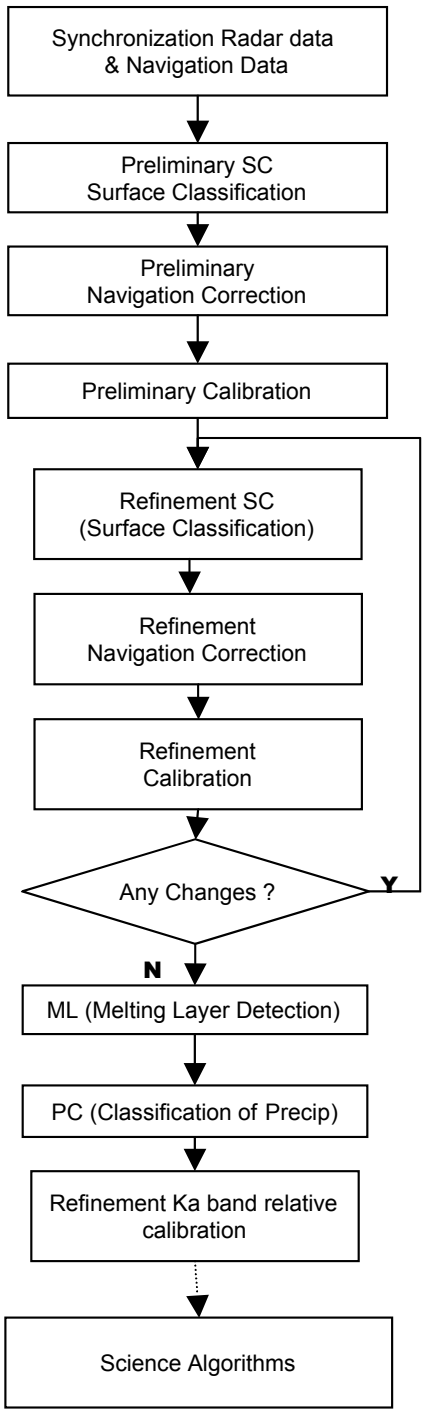

Figure 4. Figure 4. General diagram of APR-2 processing software. The algorithms SC, ML and PC are described in Section3.

2. Correction for Aircraft Motion and Navigation Errors

Correct navigation is a critical aspect in producing correct and usable airborne radar data. In particular, errors in estimating the aircraft motion, and/or the antenna angle relative to both the aircraft bearing and the earth surface result in errors in: a) correction for the aircraft motion contamination on Doppler velocity measurements, b) external calibration of the radar using the ocean surface backscattering, c) comparing/integrating with measurements obtained through other instruments. While the latter is significant only for relatively large errors (e.g., angle errors equivalent to one or more radar beamwidths), the former two are sensitive also to sub-beamwidth errors. As far as the specific configuration used for the Wakasa Bay experiment is concerned, errors in the navigation parameters occurred because of turbulence (the P-3 operates at relatively low altitude), lack of coregistration of radar data with navigation data (the latter being recorded only once per second), and uncertainty in the relative orientation of the radar reflector with respect to the aircraft reference system. Measurements obtained from the DC-8 aircraft (i.e., all experiments but the Wakasa Bay Experiment) are affected by a smaller degree of turbulence.

Navigation errors were corrected over ocean by minimizing two error functionals based on the comparison of two parameters of the radar apparent surface and the corresponding values calculated through the navigation parameters: the surface altitude and its Doppler velocity. Both functionals weigh more the measurements obtained at incidence angles smaller than 15 deg since the effects of range limitation and the resulting effects increase towards the margins of the scan.

The optimization procedure resulted in small residual errors both in roll angle (less than 0.2 deg in average) and apparent surface velocity (see Figure 5 for an example). A very small number of scans still shows larger anomalies due to occasional, short-term (i.e., less than the scanning time of 1.2 second) movements of the aircraft due to turbulence, or aircraft maneuvers.

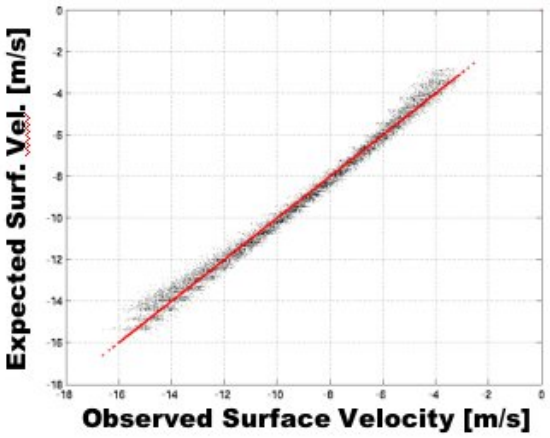

Figure 5. Comparison of observed and predicted Doppler from the ocean surface. The bias is 1 cm/s and the rms is 0.37 m/s.

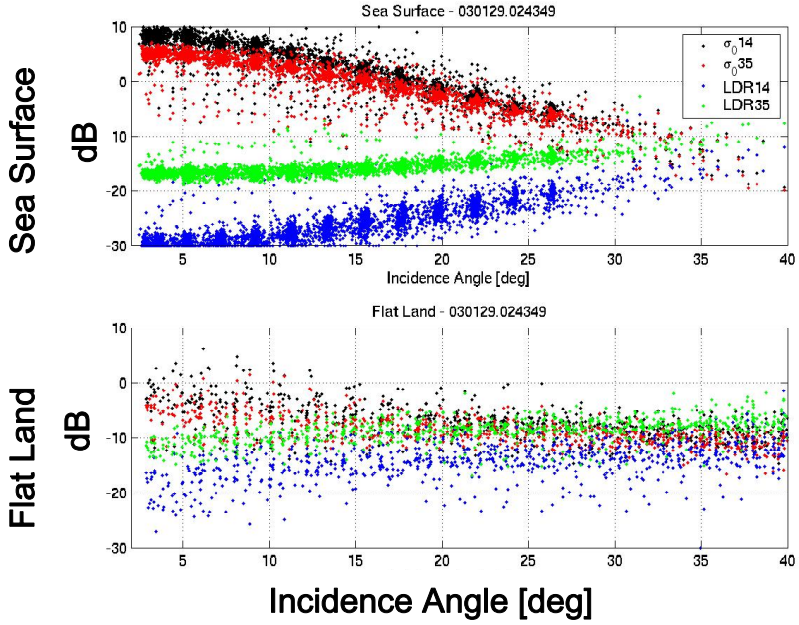

Figure 6. APR-2 measurements of the surface vs beam incidence angle. The relatively large values of LDR at Ka-band observed during the Wakasa Bay Experiment were due to higher cross-polarization leakage in the P-3 configuration: comparison of measurements of clear sea surface at Ka and Ku band allowed to correct for such leakage (see Section 1.2).

3. Classification Algorithms

Three classification algorithms complete the software package for APR-2 data processing: a Surface Classification algorithm (SC), a Melting Layer Detection algorithm (ML) and a Precipitation Classification algorithm (PC). Each one was developed to make full use of the unique set of characteristics of APR-2: high resolution (30 m vertical, ~500 m horizontal), three-dimensionality, multipolarimetry, dual-frequency and Doppler capabilities. In particular, SC and ML are necessary for accurate calibration and correction of navigation errors and are therefore embedded in the preliminary radar processing steps. Also, ML and PC provide the necessary input to the Ka-band external calibration procedure mentioned in Section 1 (see Figure 4).

3.1. Surface Classification

Surface was classified on a scan-by scan basis in two steps. Preliminary screening is performed through the Ku-band reflectivity channel alone: the cross-track profile of the apparent height of the surface is used to discriminate flat surface from rough surface (hills & mountains) and whether the aircraft was rolling or the antenna was not scanning. Cross-track scans classified as flat surface are further classified into Sea Surface or Flat Land by using reflectivity and LDR measurements at both Ku and Ka band channels and comparing them with the expected values for each incidence angle shown in Figure 6.

The output of SC is a surface index unique for each radar scan that can assume 6 values. Two values indicate ocean surface (one for aircraft in level flight, and one for aircraft not in level flight), two indicate flat land (level flight/non level flight), 1 for rough terrain/hills, and one for antenna not scanning (no classification available for the surface). As of version 3 of the APR-2 data version, the algorithm is not capable of classifying the surface within each scan (i.e., measurements taken along a coastline are classified as flat land or sea surface), and it does not fully account for the effects of strong precipitation near the surface (i.e., some misclassification occurs in areas of strong precipitation). Examples of SC outputs are visible in Figure 7 (see figure caption for color key). A secondary product of the SC algorithm is the index of the last range bin not affected by surface clutter (i.e., surface clutter to precipitation return ratio < -3 dB).

3.2. Melting Layer Detection and characterization

The ML algorithm operates iteratively a 1-D (range) multiparametric algorithm (ML1) and a 2-D (along-track and azimuth) contiguity check (ML2). In ML1 the range profile of each parameter (down to the last range bin not affected by surface clutter) is first reduced into a piecewise linear curve (linearity is interrupted at the local maxima of the second derivative of the smoothed profile). The decision tree shown in Figure 10a is applied to detect the presence of a melting layer of precipitation and its upper and lower boundaries. In the ML2 algorithm the result of ML1 for each radar beam is compared with the estimates for adjacent radar beams and with the general statistics of the Melting Layer boundaries. The result of ML2 for each radar beam is either a confirmation of ML1 estimates or a flag to discard that result and reprocess it. The two algorithms are used iteratively as follows: first ML1 is applied only to the radar beams with a surface

incidence angle less than 5 deg away from nadir, then ML2 validates/discards each result, the validated results are used to calculate the pdf of melting layer boundaries and this information is fed into ML1 to constrain the range-wise search on the beams that were not validated by ML2 and on all the beams not previously processed by ML1 (i.e., those more than 5 deg away from nadir). ML2 and ML1 are called one more time to consolidate the estimates in the off-nadir beams.

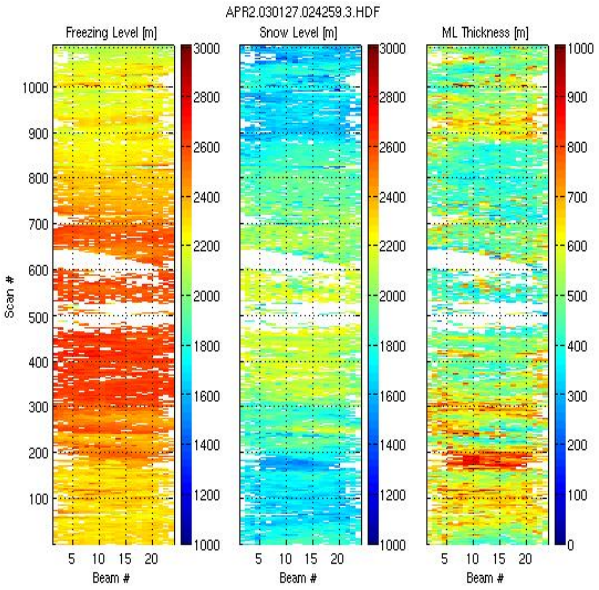

Figure 8. Main output of ML algorithm: altitude of the melting layer boundaries (note: freezing level = top, snow level = bottom) for the case shown in Figure 5. Beam number indicates the cross-track position, scan number indicates the along-track position.

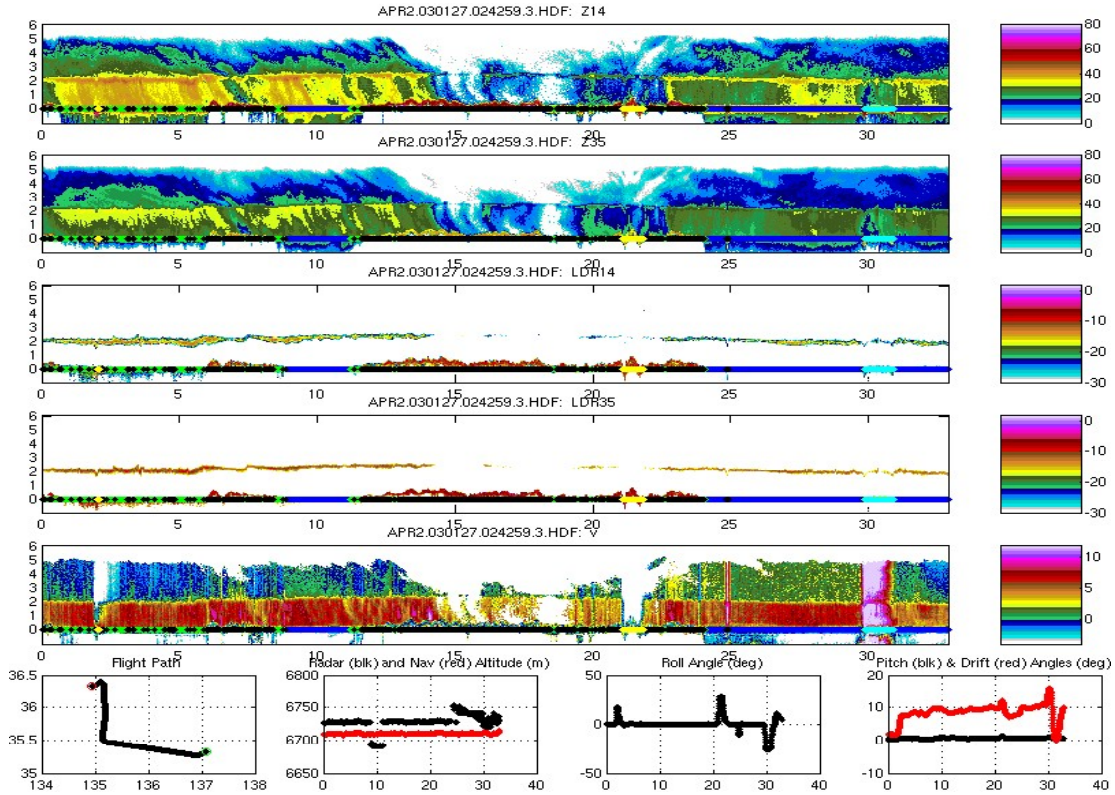

Figure 7. Stratiform precipitation over ocean and over land starting at 05:43 UTC on Jan. 19th 2003. Panels a – e: time of observation (in minutes) is shown in the horizontal axis and the altitude (in km a.s.l.) is on the vertical axis. The value of the surface index is shown at altitude 0: blue=ocean, cyan=ocean (a/c maneuvering), black=rough terrain/hill, green = flat land, yellow=flat land(a/c maneuvering). The four insets at the bottom show the navigation parameters.

The output of the ML algorithm is a set of parameters characterizing the radar signature of the melting layer of precipitation: the upper and lower boundaries of the mixed phase region, the altitude at which reflectivity and LDR reaches its maximum at each frequency within the boundaries, the thickness of each signature, the altitude at which the Doppler velocity second derivative changes and the Doppler velocity at the top and bottom of the melting layer.

3.3. Classification of Precipitation

The Precipitation Classification (PC) algorithm receives in input 3-D fields of reflectivity, LDR and Doppler (v_{14}) at Ku-band, as well as the output of ML. Radar profiles where a melting layer has been detected are classified as Stratiform Rain and the three regions of Cloud, Melting Layer and Stratiform Rain are simply obtained from the ML output. In general, each profile is analyzed through the decision tree in Figure 10b. Convection is identified either by the presence of a depolarized radar return (i.e., LDR > -30 dB) outside of the melting layer altitude region or by a difference in Doppler velocity between cloud and precipitation not consistent with the predicted increase in terminal velocity (indicated by the term $<v_{14}[Z_{14}(h)]>$ in Figure 10b). In detecting convection for all beams other than those at nadir, this differential information of Doppler measurements v_{14} is used instead of the absolute values of v_{14} in order to remove the bias introduced by the cross-track component of wind.

A 3-D morphological algorithm is applied to the 3-D field to discriminate between convection and stratiform rain, if no discrimination is possible the label 'other' is assigned. The use of a 3-D contiguity check guarantees better performances than a 2-D contiguity check (i.e., along-track and azimuth only) in regions where horizontal advection is significant (such as in the Example shown in Figure 9). At present, classification between Cloud and Snow is based only on the comparison Z_{14}-Z_{35} > 3 dBZ.

The output of PC is an index that can assume 8 values indicating: no return, cloud, stratiform precipitation, convection, snowfall, other, melting layer, weak return. An example of PC output is shown in Figure 9.

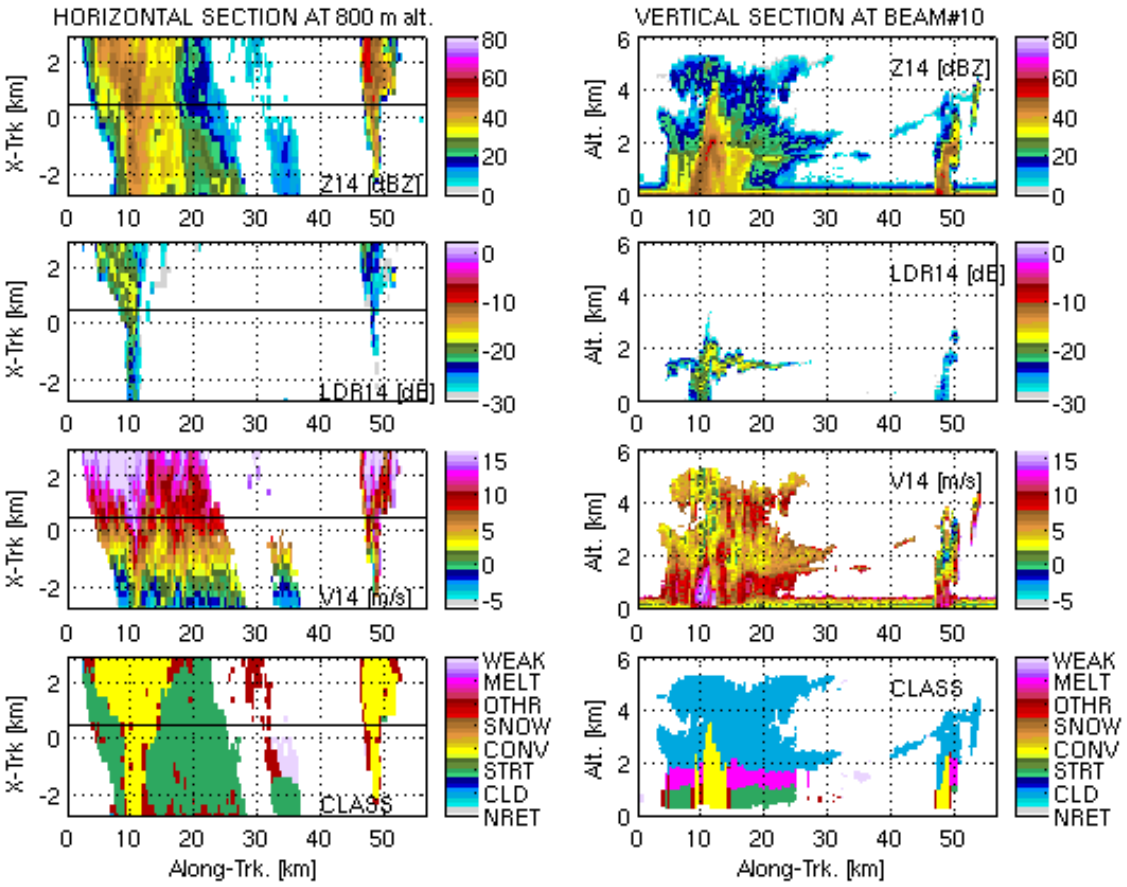

Figure 9. Example of PC output. Isolated (km 50) and embedded (km 10) convective cells observed on Jan 21st 2003 at ~35.5N 149E. Left hand panels show a horizontal section of the 3-D fields at 800 m altitude, right hand panels show a vertical section indicated by a black solid line in the horizontal section panels. Surface winds were visually estimated in the 35-40 kts range, approximately orthogonal to the line of flight: this is in good agreement with the Doppler measured cross-track wind shear shown in the horizontal section.

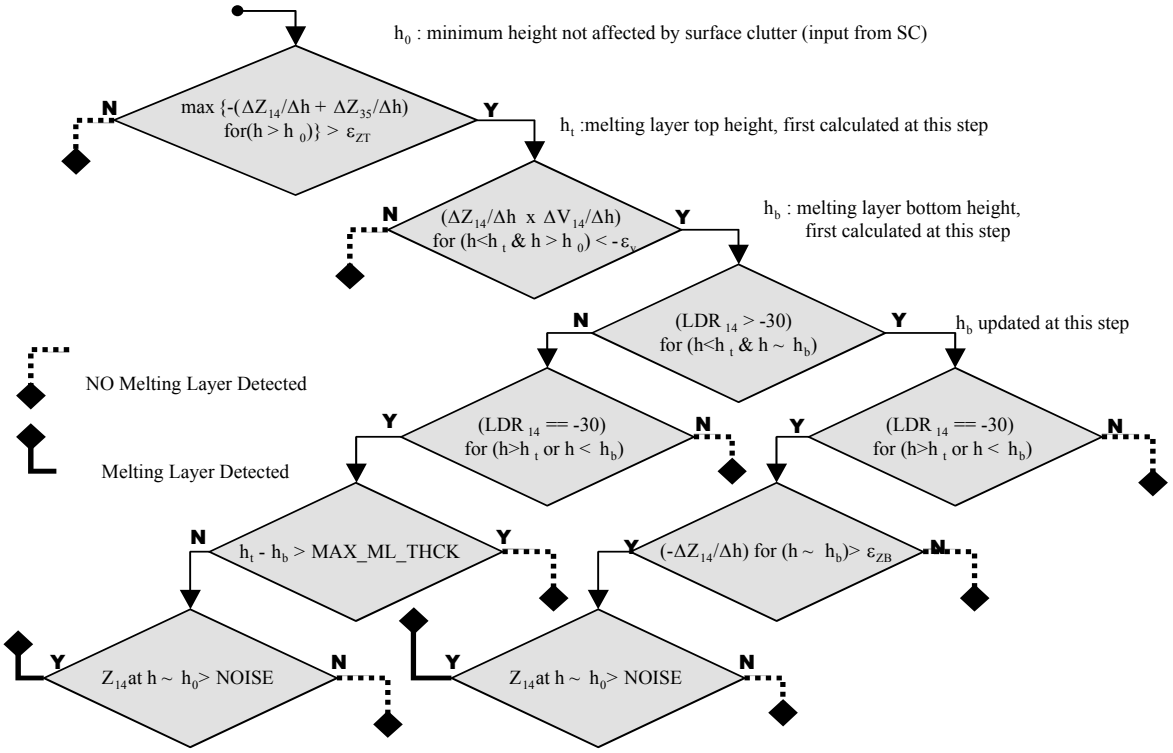

a)

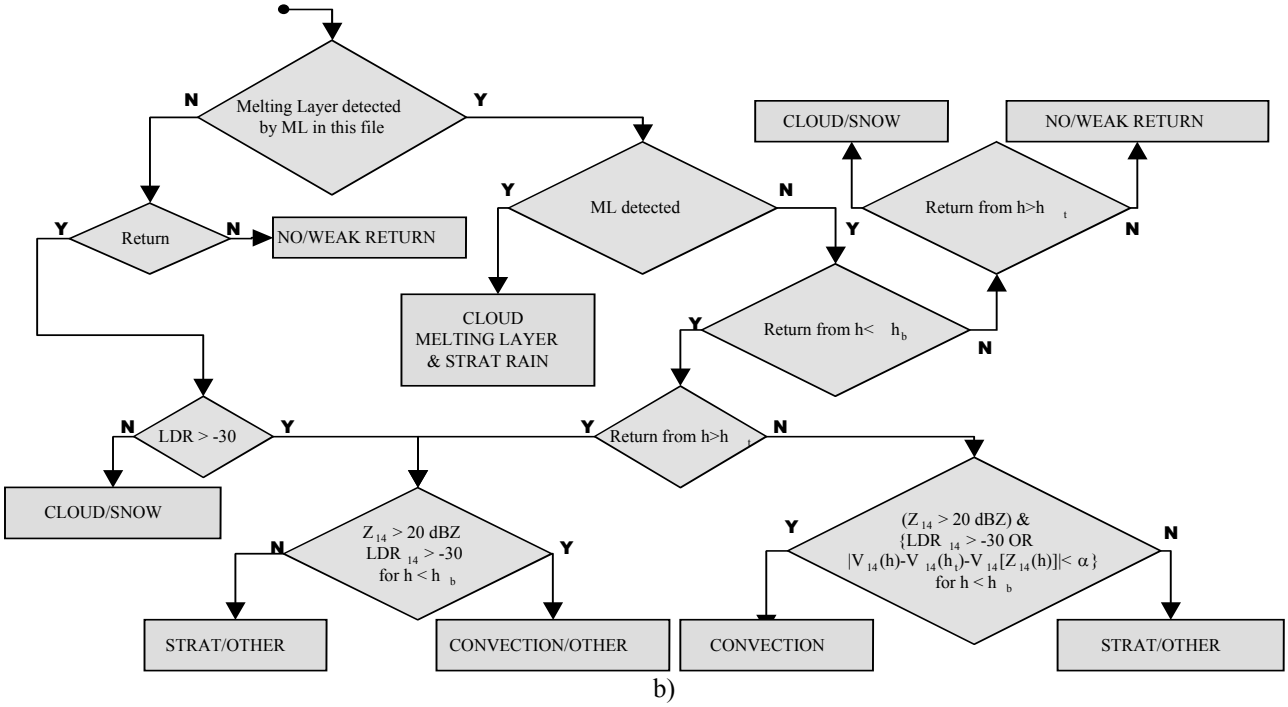

b)

Figure 10: Diagram of decision trees used in the ML1 (a) and PC (b) algorithms

CONCLUSIONS

The NASA/JPL airborne precipitation radar APR-2 collected more than 30 hours of data during the Wakasa Bay Experiment in January and February 2003. The whole dataset was processed for external calibration, correction of navigation errors and contamination of Doppler measurements by aircraft motion. Three classification algorithms have been developed for APR-2: a surface classification algorithm, a melting layer detection algorithm and a precipitation classification algorithm. All the algorithms were incorporated in the APR-2 processing software in order to provide high quality deliverables. The same software package will be used to process also all the other datasets obtained by APR-2.

ACKNOWLEDGEMENT

The research described in this paper was performed at the Jet Propulsion Laboratory, California Institute of Technology, for the AQUA/AMSR-E validation program under contract with the National Aeronautics and Space administration. The authors acknowledge the contributions of Ms. Angela Magee, Ms. Andrea Kung and Ms. Kamalah Chang in the development and implementation of the APR-2 data processing software package.

REFERENCES

1. C. Kummerow et al., “The Tropical Rainfall Measuring Mission (TRMM) sensor package,” *J. Atmos. Oceanic Technol,* vol. 15, pp. 809-817, 1998.
2. G.A. Sadowy, Berkun, A.C., Chun, W., Im, E., Durden, S.L., “Development of an advanced airborne precipitation radar”, *Microwave Journal,* vol 46, n 1, January, 2003, p 84-98.
3. E. Im et al., “Second-Generation Spaceborne Precipitation Radar, Proc. IGARSS 2000.
4. S. L. Durden, E. Im, F. K. Li, W. Ricketts, A. Tanner, and W. Wilson, ``ARMAR: An airborne rain mapping radar," *J. Atmos. Oceanic Technol*., vol. 11, no. 3, pp. 727-737, 1994.